21 September 2001

ELSEVIER

Chemical Physics Letters 345 (2001) 415–422

CHEMICAL PHYSICS LETTERS

www.elsevier.com/locate/cplett

The photodissociation of water-clustered HNO_3 studied at 193 nm by the LIF method

Qiang Li, J. Robert Huber *

Physikalisch-Chemisches Institut der Universität Zürich, Winterthurerstrasse 190, CH-8507 Zürich, Switzerland

Received 18 June 2001; in final form 2 August 2001

Abstract

We studied the photodissociation of water-clustered HNO_3 molecules at 193 nm, a process relevant in atmospheric chemistry, by generating water clusters by adiabatic expansion and doping them with HNO_3 using the pickup method. The nascent $OH(X^2\Pi)$ photofragments were probed by LIF, and the rotational state distribution in the exclusively produced vibrational ground state determined. These experiments were complemented by corresponding ones with argon and methanol clusters. The average cluster size was estimated to be $\bar{n} \sim 200$–800 depending on the compound. The results of this study are compared with those previously obtained from the photodissociation of the HNO_3 monomer. © 2001 Elsevier Science B.V. All rights reserved.

1. Introduction

The photodissociation of nitric acid HNO_3 has been well investigated, motivated mainly by the importance of this compound for atmospheric chemistry [1–3]. Following excitation into the weak, broad and structureless $n\pi^*$-absorption band at 260 nm, the major primary decay process yields $OH + NO_2$, both in their electronic ground states with a quantum yield ϕ near unity (channel (1) below) [4,5]. The nascent OH fragments have no vibrational excitation and the rotational state distribution is Boltzmann. With excitation into the strong absorption at 193 nm, the solar photolysis conditions in the stratosphere, where the 190–220 nm region is largely unfiltered by O_3, O_2 and N_2, is well reproduced. At this wavelength the primary photodissociation channels, studied by photofragment translational energy spectroscopy [6,7] and LIF [8–10] and REMPI-TOF methods [10], were found to be:

$$HNO_3 + h\nu \rightarrow OH(X) + NO_2\ (X^2A_1) \quad \Delta H^\circ = 200\ \text{kJ/mol} \quad (1)$$

$$\rightarrow OH(X) + NO_2\ (1^2B_2) \quad \Delta H^\circ = 315\ \text{kJ/mol} \quad (2)$$

$$\rightarrow O(^1D) + HONO\ (\tilde{X}^1A') \quad \Delta H^\circ = 490\ \text{kJ/mol} \quad (3)$$

$$\rightarrow O(^3P) + HONO\ (\tilde{a}^3A'') \quad \Delta H^\circ = 550\ \text{kJ/mol} \quad (4)$$

$$\rightarrow O(^3P) + HONO\ (\tilde{X}^1A') \quad \Delta H^\circ = 300\ \text{kJ/mol} \quad (5)$$

The photolysis at 193 nm is dominated by the formation of O + HONO with $\phi \sim 0.54$ [7] and $\sim$0.13 [7] for channels (3) and (4), respectively. A

* Corresponding author. Fax: +41-1-635-6838.
E-mail address: jrhuber@pci.unizh.ch (J. Robert Huber).

PII: S0009-2614(01)00915-0

minor decay path ($\phi \leqslant 0.075$) has tentatively been assigned to (5) [10]. On the other hand, the formation of $OH + NO_2$ which shows bimodal translational energy [6,7] and rotational state distributions [10] for the OH fragments has been attributed to channel (1) with $\phi \sim 0.22$ and channel (2) with $\phi \sim 0.10$ [7].

In view of the potential importance of the photodissociation of HNO_3 attached to ice particles in the stratosphere [11–14], we explored this problem in our laboratory by generating water clusters in a supersonic expansion and attaching HNO_3 to them by a pickup method [15,16]. The subsequent photodissociation was carried out at 193 nm with detection of the nascent OH ($X^2\Pi$) fragments by LIF. These experiments were complemented by corresponding experiments with argon and methanol clusters. The broad cluster size distributions were estimated to have an average size in terms of cluster molecules of $n \sim 200$–800 depending on the compound. The rotational state distribution and the average translational energy of the OH fragments emerging from the clustered HNO_3 molecules after photodissociation were measured and compared to those previously obtained from HNO_3 monomer photolysis.

2. Experiment

The apparatus used for this work is described elsewhere [17,18]. A pulsed molecular beam of HNO_3 seeded in a noble gas was generated with a specially designed corrosion resistant valve driven by a piezoelectric translator [19]. Fuming nitric acid (Merck, labeled 100%) was degassed to remove air and traces of NO_2 until it was colorless. In order to generate the cluster beams, two kind of cluster preparations were employed. In the first case the components were premixed and then subjected to supersonic expansion, in the second case a pickup technique was utilized.

Following premixing of 1% HNO_3 in Ar at a backing pressure of $\leqslant 2.4$ bar or 1% HNO_3 with 250 mbar CH_3OH in $\leqslant 2$ bar He, expansion was conducted through a pulsed valve equipped with a conical nozzle (aperture $d = 1$ mm, length 10 mm, opening angle $2\theta = 20°$) which favors cluster formation. In contrast, for cluster production by pickup the setup shown in Fig. 1 was used. First a pulsed supersonic cluster beam of either pure argon, methanol or water was generated which then was crossed by a pulsed HNO_3 monomer beam at right angle. The HNO_3-doped clusters formed in the interaction region were extracted through a skimmer into a second chamber with an additional differential pump stage. For production of the pure cluster beams we used the valve described above and 2 bar Ar, or in the case of methanol and water, 2 bar He which was guided into a flask filled with CH_3OH or H_2O at a temperature of 35 and 60 °C, respectively. The outgoing gas mixtures, possessing partial pressures of $p(CH_3OH) = 300$ mbar or $p(H_2O) = 250$ mbar, were then passed

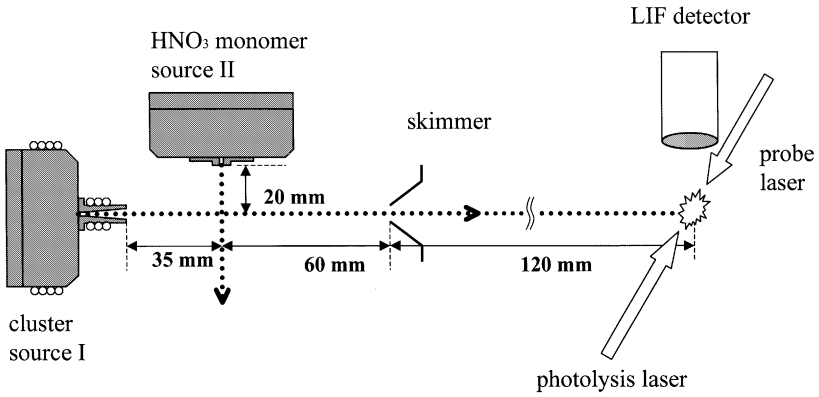

Fig. 1. Experimental setup for cluster production by the pickup method and cluster photodissociation with LIF fragment detection. The conditions for the pulsed cluster (I) and monomer (II) beams are given in the text.

through a heated tube to the pulsed valve. The latter was also heated to prevent condensation of CH_3OH or H_2O. On the other hand, the 'soft' HNO_3 monomer beam was produced by expanding a mixture of 4% HNO_3 in 300 mbar He through a pinhole aperture ($d = 0.5$ mm) attached to the piezoelectric pulsed valve. The carrier gas He will not form clusters and the low stagnation pressure prevents HNO_3 from clustering. The pulse still provides a well localized, relatively highly concentrated HNO_3 environment. In order to optimize the mixed cluster formation the distance between nozzle I and the crossing of the HNO_3 monomer beam (Fig. 1) could be adjusted (to usually about 35 mm) as well as the time delay between the opening of the pulsed valves I and II.

In our work there is no direct way to measure the cluster size distributions but a rough estimate can be given based on the work of Buck and Krohne [20] and Hagena [21]. For a pure argon expansion under the conditions used to produce Ar_nHNO_3 clusters, we obtain an average size in terms of $\overline{n} \sim 200$–400. In the cases of $(CH_3OH)_nHNO_3$ and $(H_2O)_nHNO_3$ $\overline{n}$ is expected to be in the range of $\sim$300–600 and $\sim$400–800, respectively. We expect the mixed clusters to contain only one (pickup) or a few (premixing) HNO_3 molecules; associations of the latter were not found to be important below about 8% HNO_3 concentration.

Photolysis at 193 nm was carried out with an ArF excimer laser (Lambda Physik EMG 101 MSC). The softly focussed laser beam crossed the molecular beam at right angles (Fig. 1). A counterpropagating probe laser beam recorded the nascent OH photofragments on the $A^2\Sigma^+ \leftarrow X^2\Pi$ system (vibrational bands with $\Delta v = 0$) by the LIF method. The probe laser (Lambda Physik dye laser FL2002) was pumped by an XeCl excimer laser (Lambda Physik LPX200) operated with Sulforhodamine B dye. After frequency doubling the linewidth of the laser light was 0.4 cm^{-1} between 306 and 311 nm. Fluorescence from the OH fragments was measured at right angles to the plane of the molecular and laser beams by a Hamamatsu R928 photomultiplier tube equipped with an appropriate cutoff filter. The signal was fed to a digital boxcar integrator (Stanford Research SR 250), and photodiodes monitored the photolysis and probe laser intensities to correct for shot to shot fluctuations. Since the LIF signal was found to be linear when the dissociation laser was operated in the range 3–16 mJ/cm^2, we used 5 mJ/cm^2 to safely avoid multiphoton processes in dissociation. The probe laser power density was kept at 0.1 mJ/cm^2 thus avoiding saturation effects. The Doppler profile measurements were carried out by operating the probe laser with an intracavity etalon which provided $\Delta v = 0.08 \pm 0.01$ cm^{-1}.

3. Results

3.1. Clusters by premixing

The unpolarized LIF spectra of OH ($A^2\Sigma^+ \leftarrow X^2\Pi$, $\Delta v = 0$) fragments upon 193 nm photodissociation of Ar_nHNO_3 and $(CH_3OH)_nHNO_3$ clusters generated by premixing of the components are shown in Fig. 2. No signal was detected when the wavelength of the probe laser was tuned to the position of the OH (1,1) band indicating a negligible population of OH ($v = 1$) and very probably also of higher vibrational states. From the LIF spectra we obtained the rotational state populations of the OH fragments given in Fig. 3 using standard procedures [22]. A comparison between the LIF spectra of Fig. 2a,b to that recorded from HNO_3 monomer dissociation [10] shows that the intensity of high rotational lines is considerably smaller in the former indicating rotational state relaxation in cluster dissociation.

The rotational state distribution of OH ($v = 0$) from Ar_nHNO_3 clusters (Fig. 3a), showing a maximum at $N = 2$ and extending to $N = 10$, is well described by a Boltzmann distribution (solid line) with a temperature $T_{rot} = 400 \pm 100$ K. That of the $(CH_3OH)_nHNO_3$ clusters has a maximum at $N = 1$ followed by a population decrease to $N = 8$ and fits a Boltzmann distribution with a temperature $T_{rot} = 250 \pm 150$ K (solid line in Fig. 3b). The resulting mean rotational energy $\langle E_{rot} \rangle = \sum_J P(J)E_{rot}(J)$, where $P(J)$ is the state distribution and E_{rot} the energy of a given rotational state, was found to be 290 cm^{-1} (3.5 kJ/mol) and 175 cm^{-1} (2.1 kJ/mol) for the Ar_nHNO_3 and $(CH_3OH)_nHNO_3$ clusters, respectively.

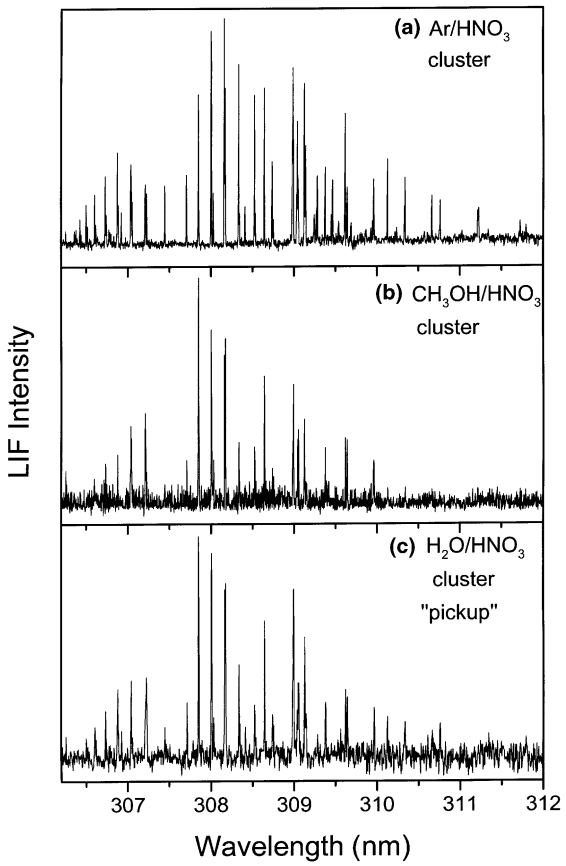

Fig. 2. Unpolarized LIF spectra of nascent OH ($A^2\Sigma^+ \leftarrow X^2\Pi$) (0,0) fragments after 193 nm photolysis of HNO_3 (a) in argon clusters (premixed), (b) in methanol clusters (premixed) and (c) in water clusters (pickup).

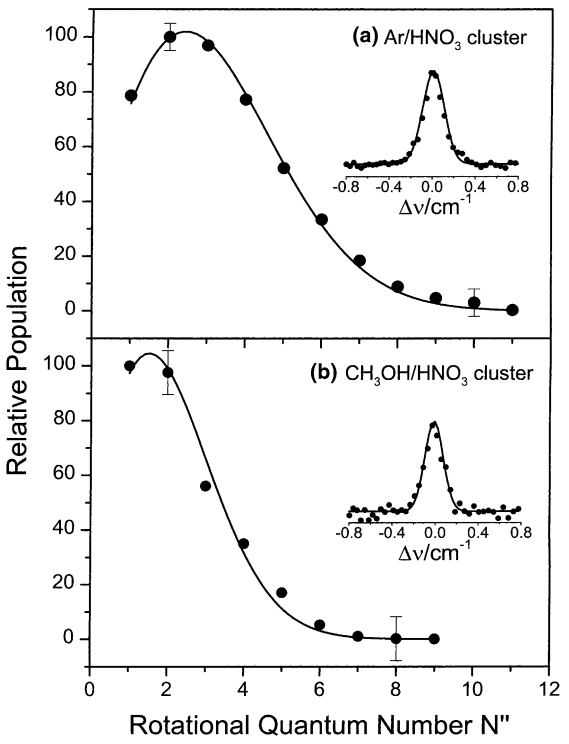

Fig. 3. Rotational state distributions of nascent OH ($X^2\Pi, v = 0$) fragments from 193 nm photolysis of HNO_3 in (a) argon and (b) methanol clusters (premixed). The solid lines represent the best fits for a Boltzmann distribution with $T_{rot} = 400$ and 250 K, respectively. The inserts show the Doppler profiles for the P_1 (2) rotational state.

Further analysis of the spectra reveal that the spin–orbit states $\Pi_{3/2}$ and $\Pi_{1/2}$ spaced by 126 cm^{-1} [23] are equally populated for both cluster systems which is also the case for the almost degenerate lambda doublet states $\Pi(A')$ and $\Pi(A'')$ as obtained from the intensities of the R and Q branches. The translational energy of the OH fragment was estimated from the Doppler width of the spectral lines $N = 2$ and $N = 6$, depicted as inserts in Fig. 3. After deconvolution with the probe laser profile, we found the Doppler width to be 0.11 ± 0.01 cm^{-1} for the argon clusters and 0.09 ± 0.01 cm^{-1} for the methanol clusters which corresponds to a mean translational energy $E_{trans}(OH) = 540$ cm^{-1} (6.5 kJ/mol or $T_{trans} \sim 500$ K) and 350 cm^{-1} (4.2 kJ/mol or $T_{trans} \sim 350$ K), respectively.

In order to study the formation of the Ar_nHNO_3 and $(CH_3OH)_nHNO_3$ clusters, we monitored the intensity of a high rotational line of the OH fragment, which is prominent in the monomer and absent in the cluster dissociation, as a function of the stagnation pressure p_0 [18,24]. Thus we selected the OH ($v = 0$) $Q_1(13)$ rotational line at the probe wavelength of 311.02 nm and obtained the results shown in Fig. 4. Changing p_0 from 0.3 to 2.4 bar of a mixture of 1% HNO_3 in Ar carrier gas results in the intensity of this rotational line (Fig. 4a) decreasing abruptly at ~0.8 bar, and assuming a constant minimum value at ~1.3 bar. This behavior is typical for a 'phase transition' associated with cluster formation [18,25,26]. A similar behavior (Fig. 4b) is observed for the

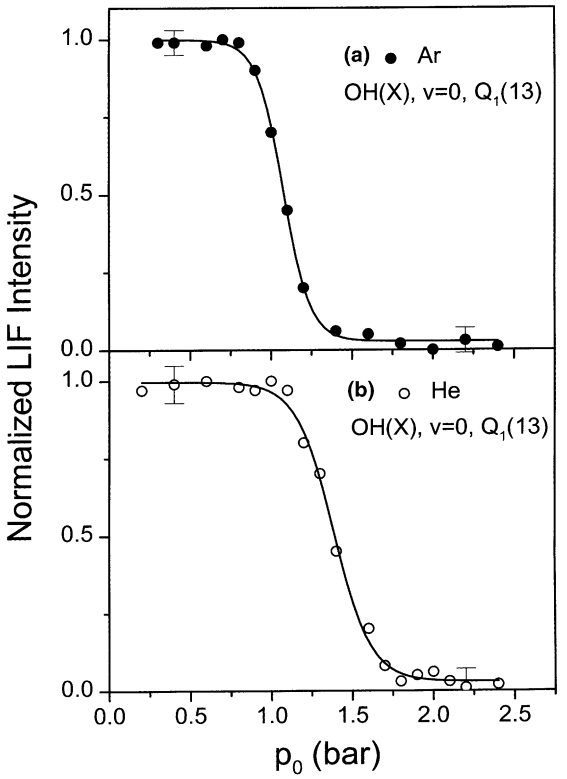

Fig. 4. Cluster formation ('phase transition') as a function of the stagnation pressure p_0 monitored by the intensity of the OH($v = 0$), $Q_1(13)$ rotational transition which is essentially absent following cluster photolysis. The expansion conditions were (a) 1% HNO_3 in argon and (b) 1% HNO_3 with 250 mbar CH_3 OH in helium.

$(CH_3OH)_nHNO_3$ system using a mixture of 1% HNO_3 in He and keeping the partial pressure of CH_3OH constant at 200 mbar. The phase transition occurs here between ~1.1 and 1.7 bar. Thus the stagnation pressures applied in the above measurements guarantee a high cluster production.

3.2. Clusters by pickup

The formation of water clusters doped with HNO_3 molecules could not be obtained by premixing the components and co-expansion through the same source. Reactions of HNO_3 with H_2O prevented application of this simple method. We therefore had to use the pickup arrangement shown in Fig. 1 where the initial preparation of very cold water clusters before the pickup of HNO_3 reduced the reactivity by hindered restructuring. This method in combination with LIF probing of the OH fragments was also applied for Ar_nHNO_3 and $(CH_3OH)_nHNO_3$ allowing us to directly compare the results of the pickup and premixing methods. Fig. 2(c) depicts the unpolarized LIF spectra recorded for OH ($A^2\Sigma^+ \leftarrow X^2\Pi$, $\Delta v = 0$) from dissociation of the water cluster. Again no evidence for the population of excited vibrational states was found. The rotational state populations of OH obtained from the line strengths in Fig. 2 are displayed in Fig. 5. The results could be well fitted by a Boltzmann distribution (solid line) with a rotational temperature of 600, 330, and 300 K for the Ar_nHNO_3,

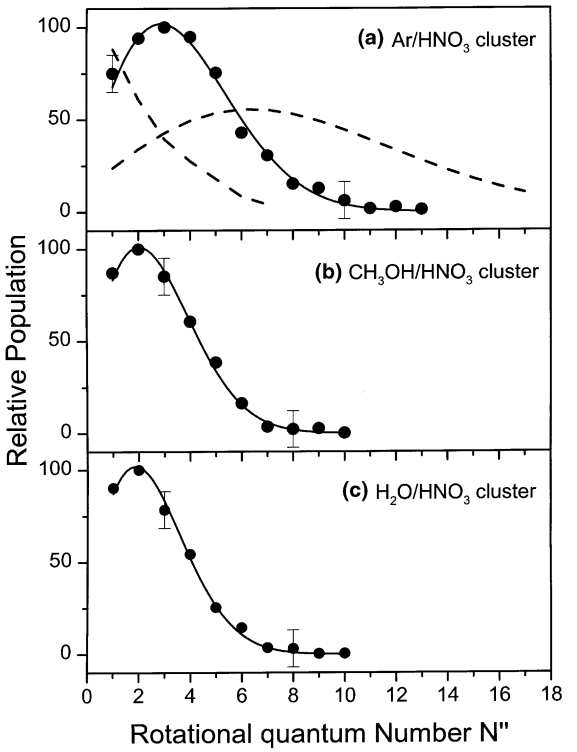

Fig. 5. Rotational state distributions of OH ($X^2\Pi, v = 0$) from 193 nm photolysis of HNO_3 (a) in argon, (b) methanol and (c) water clusters produced by pickup. The solid lines represent best fits by Boltzmann distributions with $T_{rot} = 600$, 330 and 300 K, respectively. The broken lines in (a) show the two rotational distributions from HNO_3 monomer dissociation [10].

Table 1
Photodissociation of HNO_3 monomers, and Ar_nHNO_3, $(CH_3OH)_nHNO_3$ and $(H_2O)_nHNO_3$ clusters following excitation at 193 nm[a]

	HNO_3 monomers[b]		Cluster by premixing		Cluster by pickup		
	Reaction (2)	Reaction (1)	Ar_nHNO_3	$(CH_3OH)_nHNO_3$	Ar_nHNO_3	$(CH_3OH)_nHNO_3$	$(H_2O)_nHNO_3$
T_{rot} (OH)/K	Non-thermal	2500	400	250	600	330	300
E_{rot}(OH)/cm^{-1}	120	1700	290	175	445	260	220
E_{trans}(OH)/cm^{-1}	9700	4000	540	350	830	–	–
$\Pi(A')/\Pi(A'')$	1.3±0.1	1.3±0.1	1.0±0.1	1.0±0.2	–	–	–

[a] $E_{avl} = h\nu - D_0(HO - NO_2) = 35100$ cm^{-1}.
[b] From [10].

$(CH_3OH)_nHNO_3$ and $(H_2O)_nHNO_3$ clusters, respectively. The mean rotational energy $\langle E_{rot}\rangle$ was found to be 445, 260 and 220 cm^{-1} (i.e, 5.3, 3.1 and 2.6 kJ/mol) for the Ar_nHNO_3, $(CH_3OH)_nHNO_3$ and $(H_2O)_nHNO_3$ clusters, respectively. In the case of the argon cluster the Doppler profile of OH rotational lines were also examined. The width was found to be 0.14 ± 0.02 cm^{-1} which corresponds to a mean translational energy $E_{trans}(OH) = 830$ cm^{-1}(~ 10 kJ/mol or $T_{trans} \sim 800$ K). These findings are summarized in Table 1 and compared with previously reported results from the photodissociation of HNO_3 monomer [10].

4. Discussion

The rich photochemistry of the nitric acid monomer after excitation at 193 nm is summarized by the five primary dissociation channels given in Section 1. Two of these decay processes lead to the products $OH + NO_2$ and three to $O + HONO$ involving different electronic states. Because we exclusively probed the OH fragment in the present cluster study, we are confined to investigating channels (1) and (2). These two OH channels were found to differ not only in their translational energy distributions [6,7] but also in their rotational state distributions [10]. Thus the OH fragments with the electronically excited and stable counterfragments $NO_2(1\,^2B_2)$ of channel (2) possess a non-statistical rotational state distribution with low excitation ($N < 7$) while OH with $NO_2(X\,^2A_1)$ in the ground state (1) shows a broad Boltzmann distribution ($N < 18$) with $T_{rot} = 2500$ K, as reproduced in Fig. 5a by broken lines.

HNO_3 photodissociation in a cluster environment reveals for both preparation modes a single and statistical OH rotational distribution described by a rotational temperature between 250 and 600 K (Figs. 3 and 5 and Table 1) depending on the nature of the cluster. Again only OH fragments in the vibrational ground state are formed, but in contrast to the monomer dissociation [9,10], the lambda doublet states are equally populated. In general the rotational as well as the translational excitation of OH are strongly relaxed in our cluster dissociation as compared to that of

the monomer [6,7,10,27]. The clusters prepared by pickup show a higher T_{rot} than those generated by premixing (Ar_nHNO_3: 600 and 400 K, $(CH_3OH)_nHNO_3$: 330 and 250 K, respectively). Since the stagnation pressure is lower and the chamber pressure higher for beam II than for beam I (Fig. 1) it is conceivable that this effect is caused by a slight warm up of the clusters after pickup thus assuming the interaction between the HNO_3 molecule and the cluster to be temperature dependent. Alternatively, it could arise from a less constrained surface site of HNO_3 after pickup than that associated with the premixing preparation. The photodissociation of strongly 'bonded' and even partly or fully caged HNO_3 molecules has been found to lead to substantially relaxed and often thermalized fragments, particularly with respect to the rotational and translational degrees of freedom [17]. In this context it might not be surprising that among the pickup clusters, $(H_2O)_nHNO_3$ yields the lowest T_{rot} (Table 1). The binding forces between HNO_3 molecules and the water cluster, being dipole–dipole interaction and hydrogen bonding, are expected to be the strongest among the present cluster systems.

While decay paths (1) and (2) proceeding to OH products show different rotational state distributions in the monomer, the single thermalized distribution observed in all our cluster systems might suggest that only one OH channel, probably decay path (1) with the lowest ΔH° value, is important in cluster dissociation. However, the broad cluster size distribution inherent in our preparation techniques gives rise to different environments for the HNO_3 molecules and thus to a distribution of interaction strengths between HNO_3 and the cluster. A distinction of different rotational state distribution of the ejected photoproduct OH may under these condition no longer be feasible.

5. Conclusion

The photochemistry of the HNO_3 molecule, an important source of OH radicals and NO_2 in the stratosphere, has been well studied at 193 nm and five reaction channels have been identified. The main goal of the present investigation was to extend this work to HNO_3 in or on water clusters, a system relevant to atmospheric chemistry. For the first time we produced these clusters using a pickup source and photolysed the mixed clusters at 193 nm detecting the OH ($X^2\Pi$) fragments by LIF. Complementary investigations were carried out with argon and methanol clusters, where also the preparation method by premixing of the components was applied. In contrast to the monomer, the cluster photodissociation was found to generate OH in only a single and thermalized rotational state distribution and the rotational as well as translational fragment excitation is greatly relaxed. Thus the reduced internal energy of this fragment, which is also expected for its counterfragment NO_2, makes consecutive reactions of these species involving an activation energy less probable.

Acknowledgements

Support of this work by the Schweizerischer Nationalfonds is gratefully acknowledged. We thank Dr. Robert Carter and Rolf Pfister for technical assistance and PD Dr. P. Willmott for critically reading the manuscript.

References

[1] G. Brasseur, S. Solomon, Aeronomy of the Middle Atmosphere, Reidel, Dordrecht, 1986.
[2] S. Solomon, Nature. 347 (1990) 347.
[3] J.B. Burkholder, R.K. Talukdar, A.R. Ravishankara, S. Solomon, J. Geophys. Res. D98 (1993) 22937.
[4] H.S. Johnston, S.-G. Chang, G. Whitten, J. Phys. Chem. 78 (1974) 1.
[5] G.S. Jolly, D.L. Singleton, D.J. McKenney, G. Paraskevopoulos, J. Chem. Phys. 84 (1986) 6662.
[6] P. Felder, X. Yang, J.R. Huber, Chem. Phys. Lett. 215 (1993) 221.
[7] T.L. Myers, N.R. Forde, B. Hu, D.C. Kitchen, L.J. Butler, J. Chem. Phys. 107 (1997) 5361.
[8] A.A. Turnipseed, G.L. Vaghjiani, J.E. Thompson, A.R. Ravishankara, J. Chem. Phys. 96 (1992) 5887.
[9] G.-H. Leu, C.-W. Hwang, I.-C. Chen, Chem. Phys. Lett. 257 (1996) 481.
[10] Q. Li, R.T. Carter, J.R. Huber, Chem. Phys. Lett. 334 (2001) 39.

[11] D. Salcedo, L.T. Molina, M.J. Molina, J. Phys. Chem. A 105 (2001) 1433.
[12] M.A. Zondlo, S.B. Barone, M.A. Tolbert, J. Phys. Chem. A 102 (1998) 5735.
[13] J.P. Devlin, N. Uras, M. Rahman, V. Buch, Israel J. Chem. 39 (1999) 261.
[14] A.E. Waibel, Th. Peter, K.S. Carslaw, H. Oelhaf, G. Wetzel, P.J. Crutzen, U. Pöschl, A. Tsias, E. Reimer, H. Fischer, Science 283 (1999) 2064.
[15] T.E. Gough, M. Mengel, P.A. Rowntree, G. Scoles, J. Chem. Phys. 83 (1985) 4958.
[16] C.P. Schulz, R. Haugstätter, H.-U. Tittes, I.V. Hertel, Phys. Rev. Lett. 57 (1986) 1703.
[17] E. Kades, M. Rösslein, U. Brühlmann, J.R. Huber, J. Phys. Chem. 97 (1993) 989.
[18] E. Kades, M. Rösslein, J.R. Huber, J. Phys. Chem. 98 (1994) 13556.
[19] M.-A Thelen, P. Felder, J.R. Huber, Chem. Phys. Lett. 213 (1993) 275.
[20] U. Buck, R. Krohne, Phys. Rev. Lett. 73 (1994) 947.
[21] O.F. Hagena, Rev. Sci. Instrum. 63 (1992) 2374.
[22] J. Luque, D.R. Crosley, LIFBASE: Database and spectral simulation program (Version 1.5), SRI International Report MP 99-009, 1999.
[23] G.H. Dieke, H.M. Crosswhite, J. Quant. Spectrosc. Radiat. Transfer 2 (1962) 97.
[24] J.B. Anderson, in: P.P. Wegener (Ed.), Molecular Beams and Low Density Gas Dynamics, Marcel Dekker, New York, 1974, p. 1.
[25] K. Bergmann, J.R. Huber, J. Phys. Chem. A 101 (1997) 259.
[26] C.J. Kreher, R.T. Carter, J.R. Huber, J. Chem. Phys. 110 (1999) 3309.
[27] J. Schlütter, K. Kleinermanns, Chem. Phys. Lett. 192 (1992) 94.